


Gravitational waves from neutron stars: detection prospects and inferences for two distinct types of remnants

Lecture 3 - Core Collapse Supernovae

José Antonio Font

Universitat de València

www.uv.es/virgogroup 



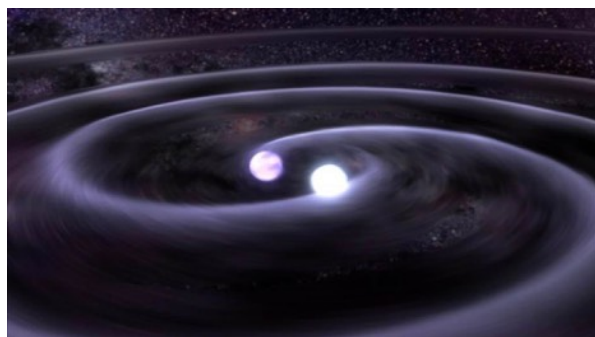
Outline

- Motivation
- LVK searches of GW from CCSN
- Proto-neutron star asteroseismology
- Rapidly-rotating progenitors
- Detection prospects and inferences

LIGO-Virgo-KAGRA physics program

Transient GW signals

Compact Binary Coalescences (CBC)
modelled

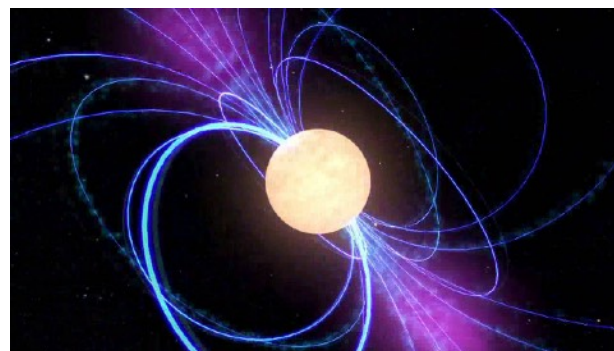


Bursts (e.g. supernovae) unmodelled

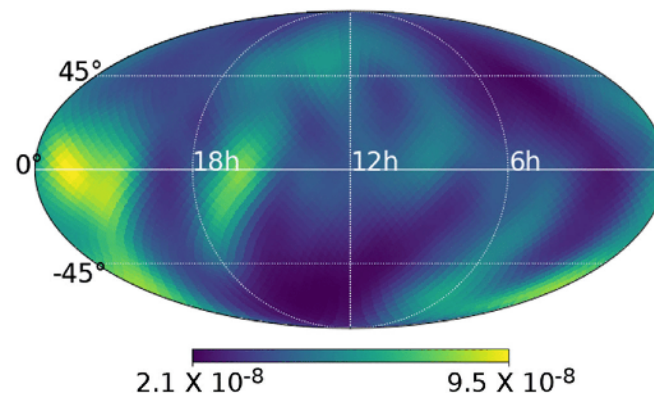


Long(er) duration GW signals

Continuous waves
(e.g. rotating neutron stars)



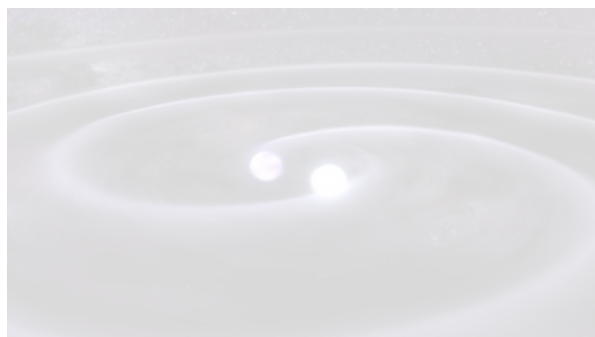
Stochastic GW background



LIGO-Virgo-KAGRA physics program

Transient GW signals

Compact Binary Coalescences (CBC)
modelled

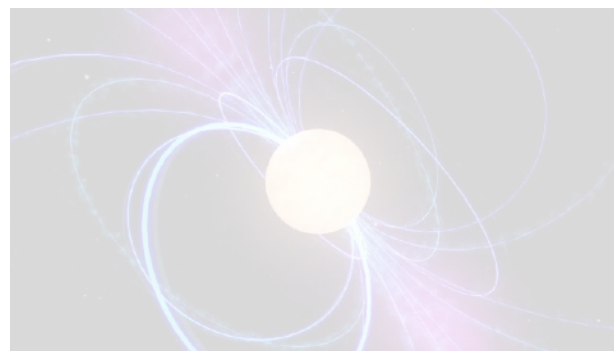


Bursts (e.g. supernovae) **unmodelled**

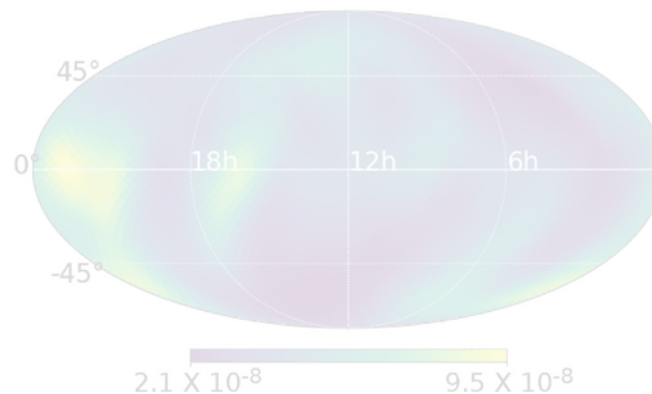


Long(er) duration GW signals

Continuous waves
(e.g. rotating neutron stars)



Stochastic GW background



Motivation

Hours after the collapse of the core shock breaks through stellar surface. Supernova explosion is then seen as an EM phenomenon (light curve).

Light curve is an “echo” of supernova driving engine. Yields indirect information about core collapse.

Two complementary methods to look at the “heart” of the supernova:

- **Neutrinos**: seconds after collapse. Tradeoff: flux decays with square of distance. Only for Galactic CCSN.
- **Gravitational waves**: decouple from matter directly after generation. In sync with core collapse. Advantage: amplitude decays linearly with distance. Extragalactic CCSN may be detectable in the future.

Difficulties:

- despite a CCSN is a very energetic event ($E_{\text{bin}} \sim 10^{53}$ erg) the deformation of spacetime and the GW amplitude is fairly small ($E_{\text{GW}} < 10^{-6} E_{\text{bin}}$). Limits realistic detectability prospects to Galactic CCSN.
- GW signals from CCSN are quite complex (unmodelled, stochastic component). NR simulations badly needed.

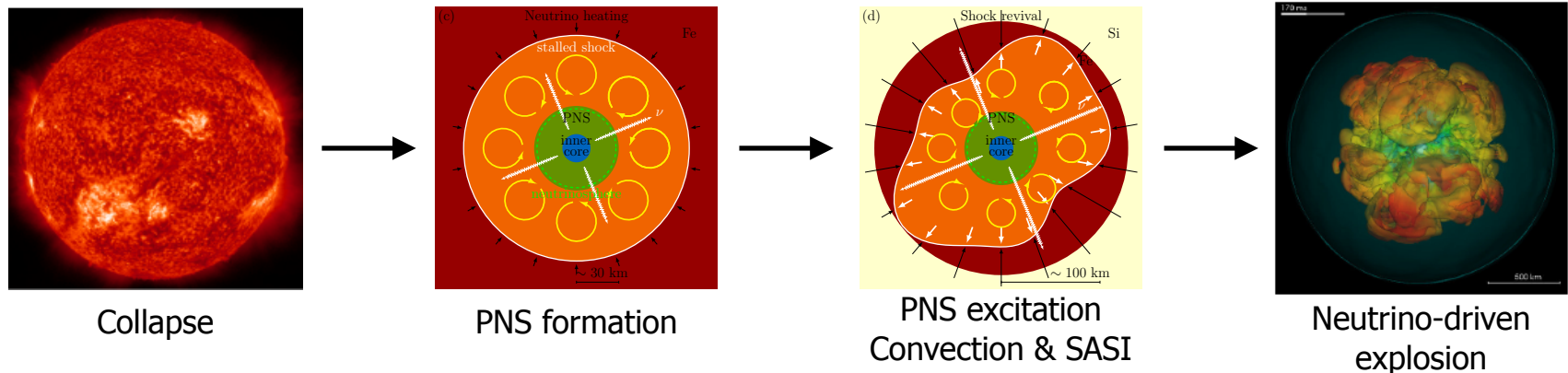
Motivation

Core-Collapse Supernovae (CCSN) are a prime source of gravitational waves. Their typical frequencies make them perfect targets for ground-based detectors. A successful detection could potentially:

- Reveal underlying **explosion mechanism** through analysis of the waveform.
- Reveal properties of progenitor and/or new-born **PNS**.

CCSN progenitors:

- massive stars 8-100 M_{sun}
- Non-rotating (>99%)
([Li+ 2011](#), [Chapman+ 2007](#))
- Observable within ~ 10 kpc
([Gossan+ 2015](#), [Powell & Müller 2018](#))
- Rare events: 1/30 yr in our Galaxy ([Adams+ 2013](#))



LVK searches of GW from CCSN

GW searches from CCSN always regarded as an **essential activity in the LVK physics program**.

First searches initiated in 2016 with Initial LIGO and Initial Virgo detectors (and GEO600).

[A First Targeted Search for Gravitational-Wave Bursts from Core-Collapse Supernovae in Data of First-Generation Laser Interferometer Detectors](#) Phys. Rev. D 94, 102001 (2016)

GW data coincident with **2 CCSN** observed optically in 2007 and 2011 (**within 15 Mpc**).

Three families of artificial GW waveforms injected into the data:

- fully (2D & 3D) **numerical simulations** of CCSN events (stochastic waveforms)
- Waveforms from **semi-analytical** calculations for models of **extreme** CCSN emission (known shape; bar-mode deformation, torus fragmentation instability)
- **Phenomenological** sine-gaussian waveforms (to probe specific combinations of signal frequency and time intervals; allows to compute upper limits on GW energy).

No GW were found, **Upper limits** on the amount of GW energy that could have been emitted by the two supernovae computed ($\sim 10^{-1} \text{ Mc}^2$ at low frequencies to $\sim 10 \text{ Mc}^2$ above 1 kHz).

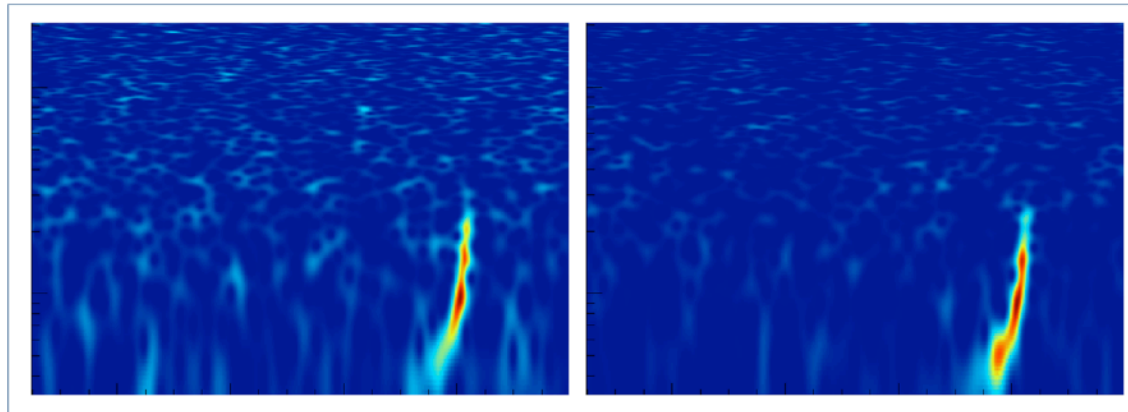
Initial searches could not constrain or exclude any of the CCSN models considered.

LVK searches of GW from CCSN

Searches not based on matched filtering (as CCSN are unmodelled GW sources)

Typical ingredients of an unmodelled search pipeline:

1. Cross-correlation of data from pairs of detectors.
2. Excess power analysis, usually coherent combinations of data from several GW detectors.
3. Look for a signal in the sensitive band ($\sim 20 - 2000$ Hz) with duration from ~ 1 ms to ~ 1 s.



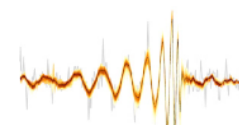
Some popular LVK CCSN search pipelines:



Coherent Wave Burst (cWB)
gwburst.gitlab.io



X-pipeline

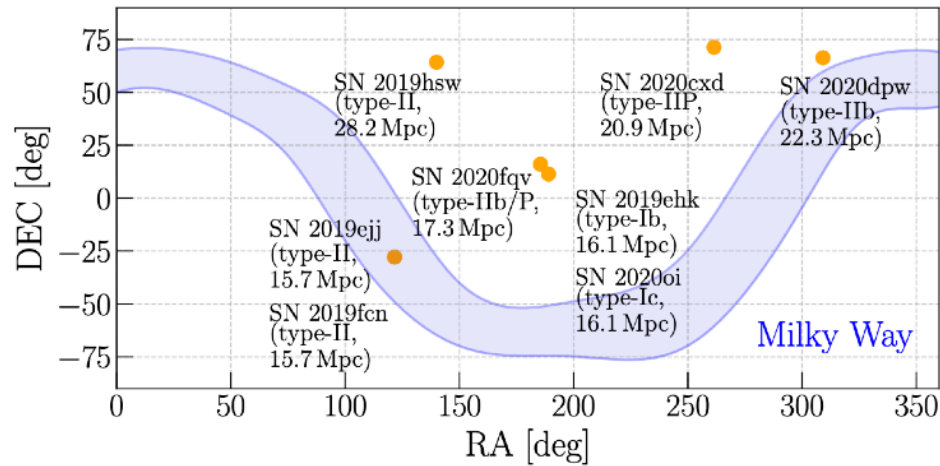


BayesWave

docs.ligo.org/lscsoft/bayeswave

O3 searches of GW from CCSN

Search for GW transients associated with **8 CCSN** observed optically **within 30 Mpc** during O3



[Szczepanczyk et al, arXiv: 2305.16146](#)

No GW association identified (not unexpected).

Analysis on detection efficiency for a variety of possible GW emission mechanisms in CCSN: neutrino-driven, magneto-rotational, BH formation, QCD phase transitions, extreme models (long-lasting bars).

New upper limits on distance reach of searches, GW energy and luminosity, and PNS ellipticity.

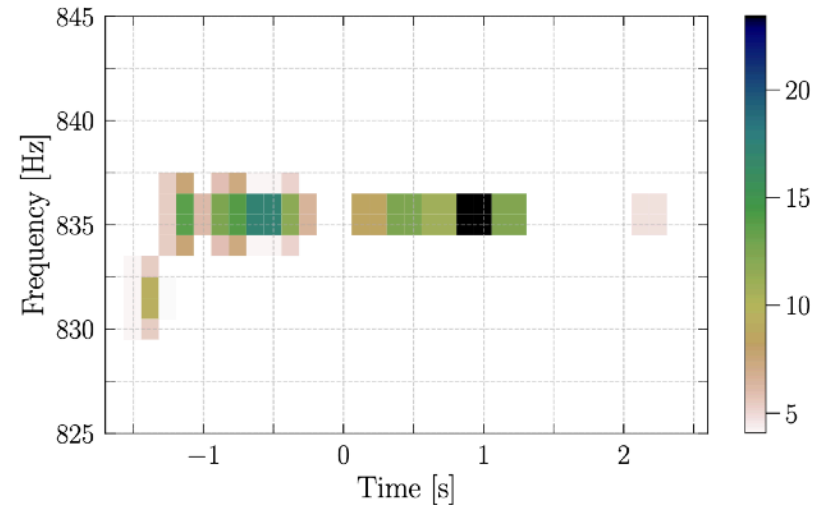
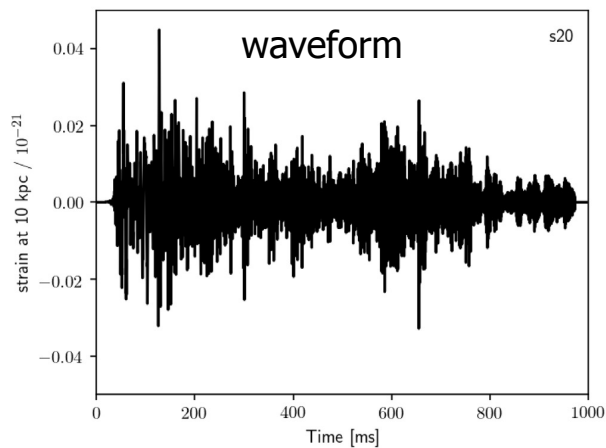


FIG. 5. SN 2020fqv loudest event with a 2.8σ detection significance. The data quality investigations show that this event is most likely of an instrumental origin.

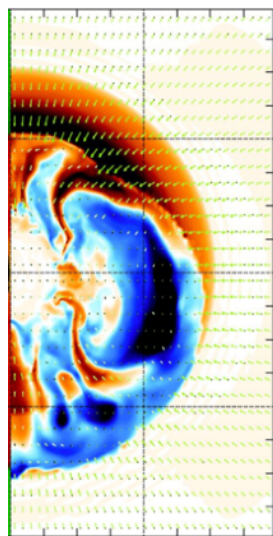
PNS asteroseismology

Gravitational waves from PNS oscillations

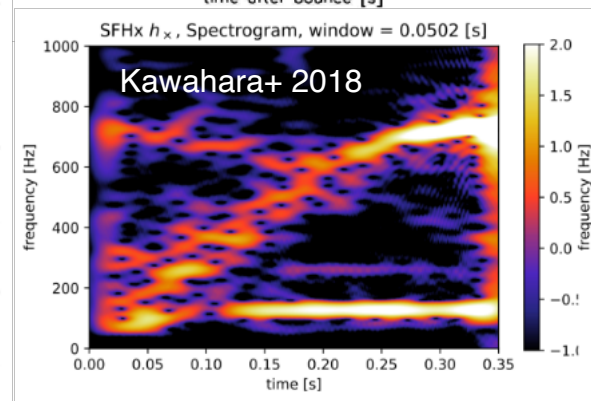
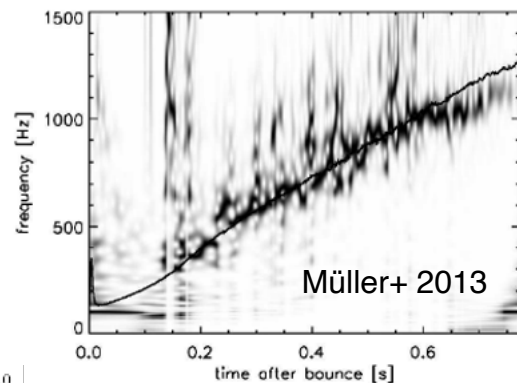
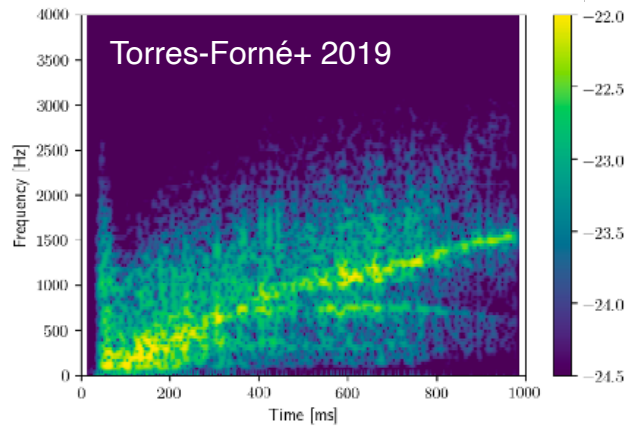
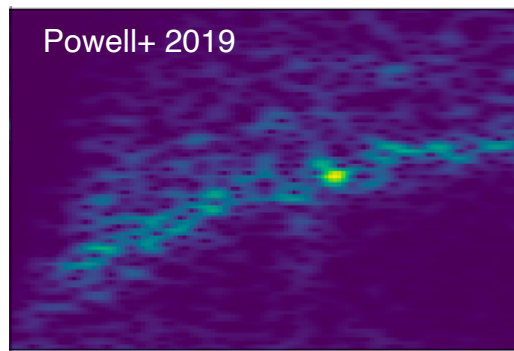


- Highly stochastic GW signal
- Frequencies evolve with time (g-modes, SASI)

spectrograms



Numerical simulation
(Obergaullinger+ 2013)



arch-shaped features observed by different groups (multiple codes)

PNS oscillations

Linear perturbations of a spherical background yields an **eigenvalue problem**.

Simplified background (TOV models):

[Reisenegger & Goldreich 1992](#), [Ferrari et al 2003, 2004](#), [Passamonti et al 2005](#), [Krüger et al 2015](#), [Camelio et al 2017](#), [Sotani et al 2017](#), ...

Dynamical background from numerical simulations of CCSN:

[Torres-Forné et al 2018, 2019a,b](#), [Morozova et al 2018](#), [Radice et al 2019](#), [Sotani et al 2019a,b](#), [Westernacher-Schneider 2019](#), [Mori et al 2023](#), [Wolfe et al 2023](#) ...

Our numerical code “**GREAT**” (General Relativistic Eigenmode Analysis Tool)

www.uv.es/cerdupa/codes/GREAT

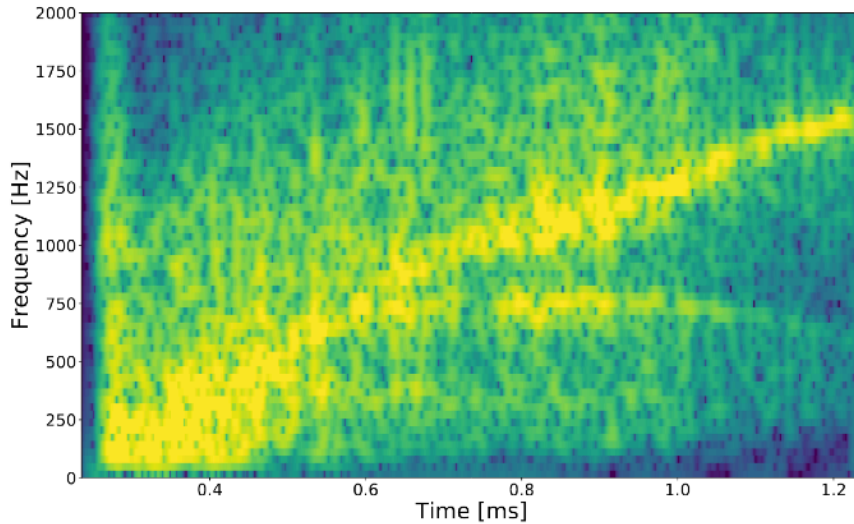
[Torres-Forné et al 2018, 2019a,b](#)

- Background from simulations
- GR formalism including space-time perturbations (lapse and conformal factor)
- Global treatment (PNS + shock)

GREAT currently being upgraded to incorporate **new solvers** (spectral methods and PINNs) and **advection terms** (accreting background, relevant for p-modes and SASI).

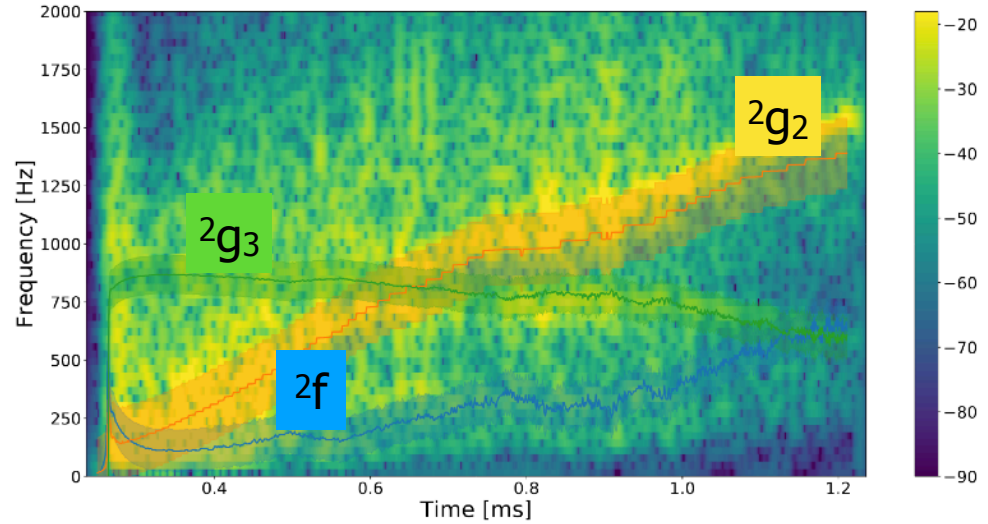
Future extensions to account for rotating stars (rotation correction to g/f/p-mode frequencies).

Gravitational waves from PNS oscillations



GW spectrogram from a $20M_{\text{sun}}$ progenitor (Cerdá-Durán+ 2013)

Torres-Forné+ 2019b



Features in spectrograms can be matched to specific PNS eigenmodes.

- **p-modes** and **f-mode**.

Fundamental p-mode.

Restoring force is pressure. $f \propto c_s \propto \sqrt{\bar{\rho}} \propto \sqrt{\frac{M}{R^3}}$

$$L^2 \approx c_s^2 \frac{l(l+1)}{r^2}$$

- **g-modes**

Gravity modes.

Restoring force is buoyancy.

$$N^2 \approx \frac{\partial \Phi}{\partial r} \frac{1}{\rho} \left(\frac{1}{c_s^2} \frac{\partial P}{\partial r} - \frac{\partial \rho}{\partial r} \right)$$

$$f \propto \frac{M}{R^2} \times \sqrt{\frac{(\Gamma - 1)m_n}{\Gamma k_b T}}$$

- Which one is the dominant mode?
- How does it depend on PNS properties?

—————> PNS asteroseismology

Quasi-universal relations

The **time-frequency relations (fits)** of excited PNS modes are **quasi-universal**, as they do not depend on the EoS, progenitor star, or neutrino treatment.

Those relations provide the potential to be used for parameter inference once actual GW observations from CCSN become available.

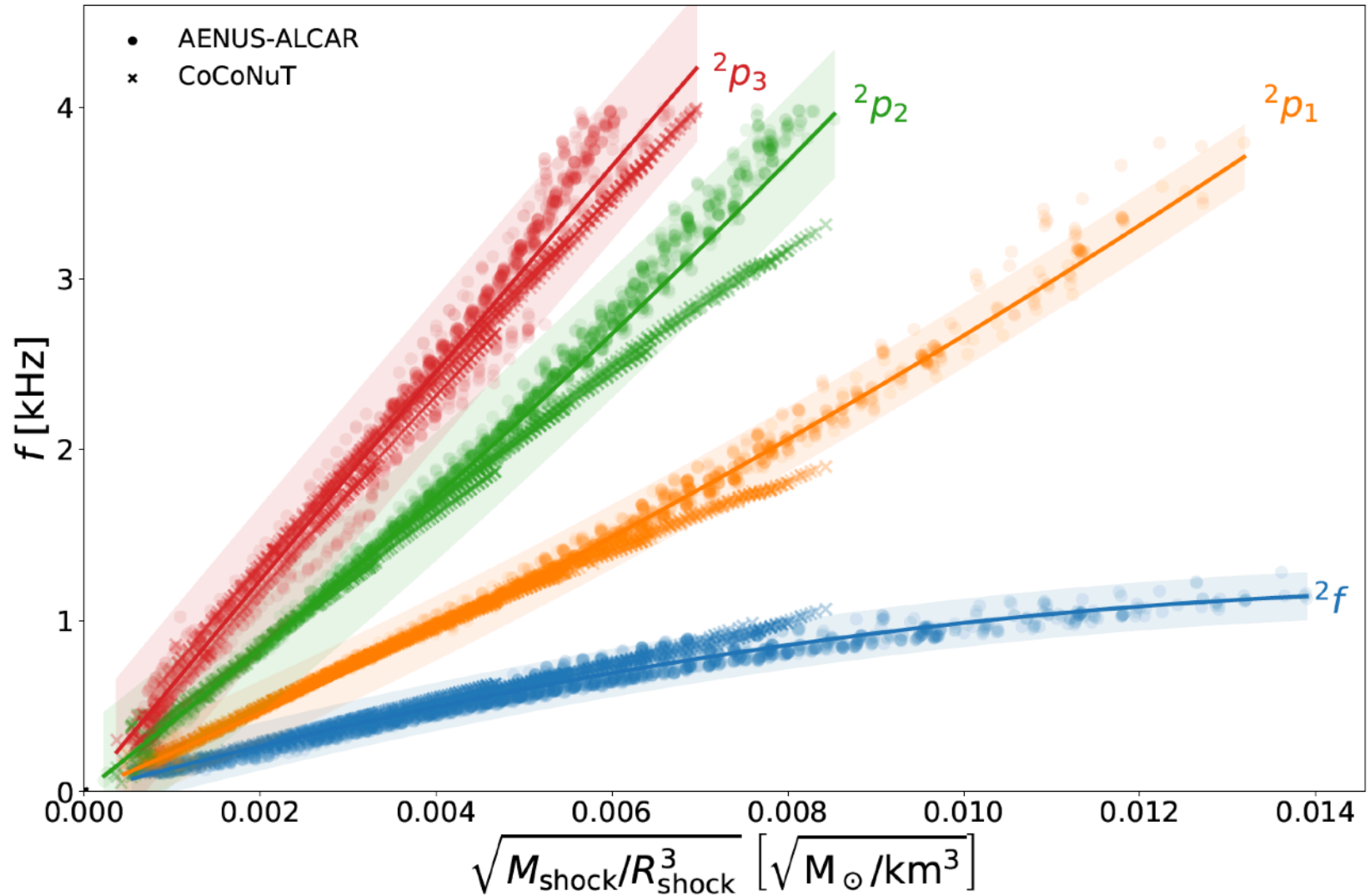
- 25 1D simulations
- 2 codes: AENUS-ALCAR ([Obergaullinger 2008](#); [Just+ 2015](#)) & CoCoNuT ([Dimmelmeier+ 2005](#))
- 6 EoS: LS220, Gshen-NL3, Hshen, SFHo, BHB- Λ , Hshen- Λ
- 8 progenitors: 11.2 - 75 M_{sun}

• fits $f = a + bx + cx^2 + dx^3$

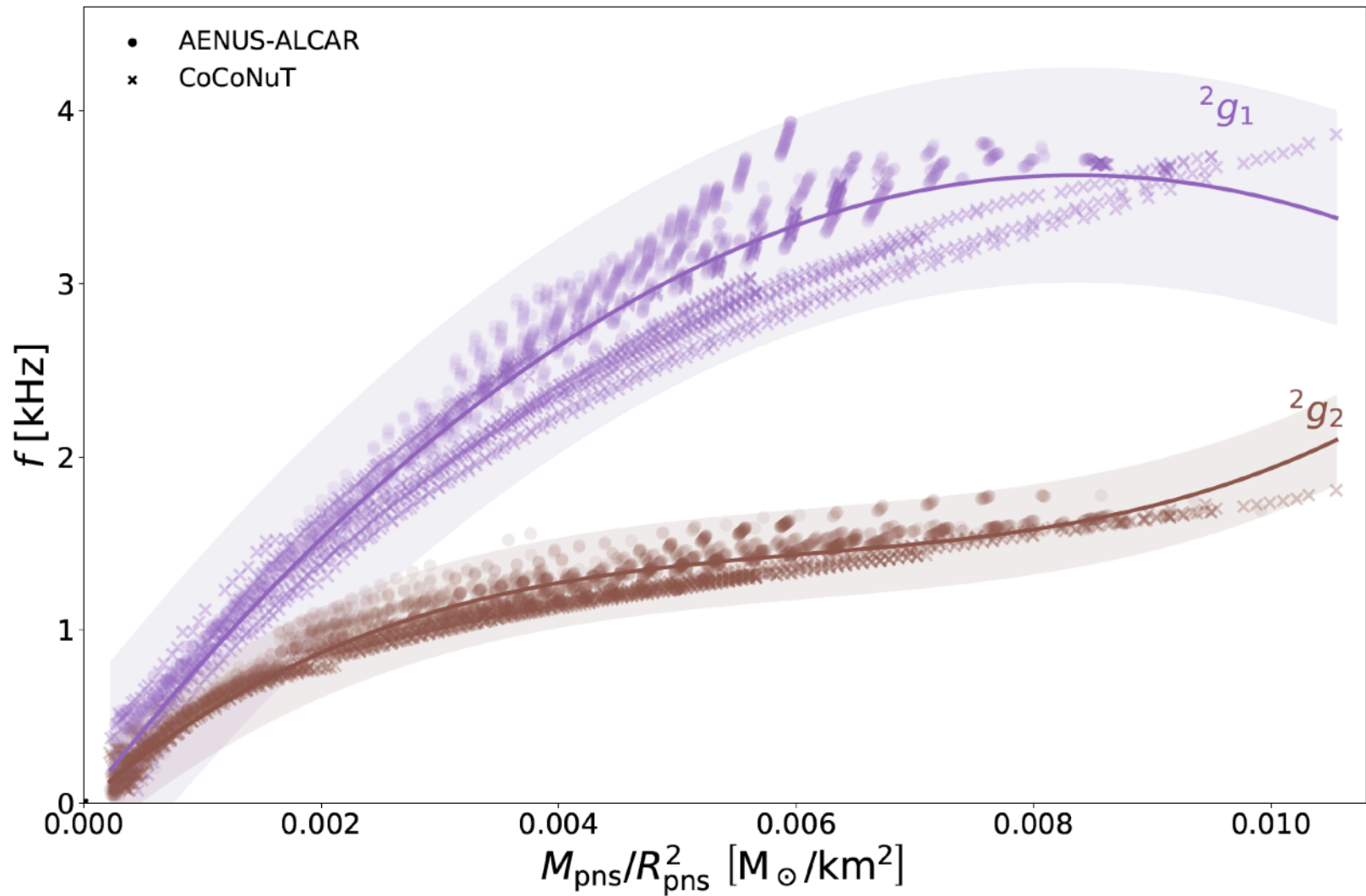
$$x = \sqrt{\frac{M_{\text{shock}}}{R_{\text{shock}}^3}} \quad x = \frac{M_{\text{PNS}}}{R_{\text{PNS}}^2}$$

f-mode and p-modes g-modes

Quasi-universal relations

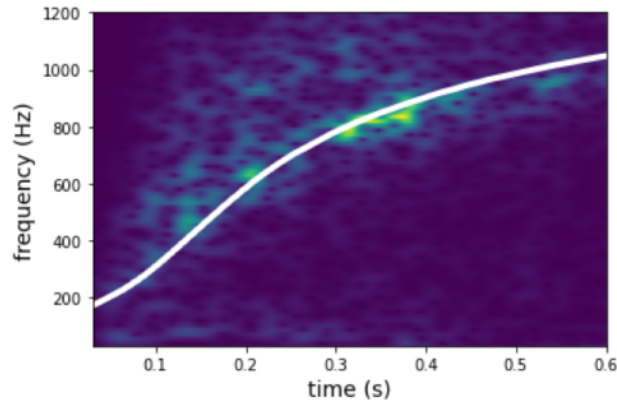


Quasi-universal relations



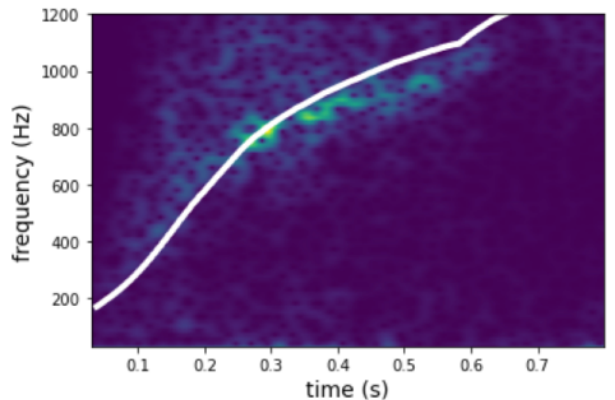
Quasi-universal relations - 3D models by Powell

2g_2 mode evolution



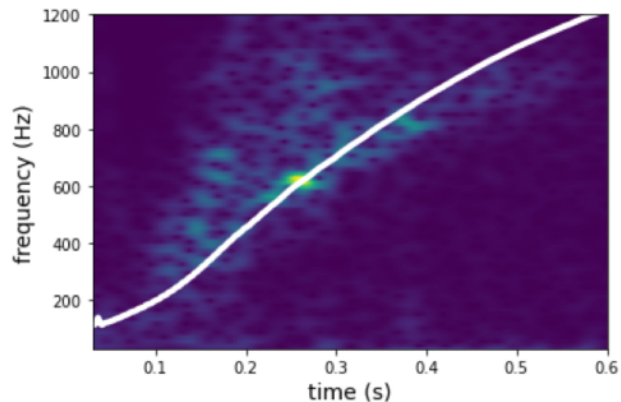
Model He3.5 (Powell & Müller 2018)

Ultra-stripped star evolved from a helium star with an initial mass of $3.5 M_{\text{sun}}$ (Tauris+ 2015)



Model s18 (Powell & Müller 2018)

Solar metallicity progenitor star with a ZAMS mass of $18 M_{\text{sun}}$.



Model y20 (Powell & Müller 2020)

$20 M_{\text{sun}}$, non-rotating, solar metallicity helium (Wolf-Rayet) star from Yoon (2017)

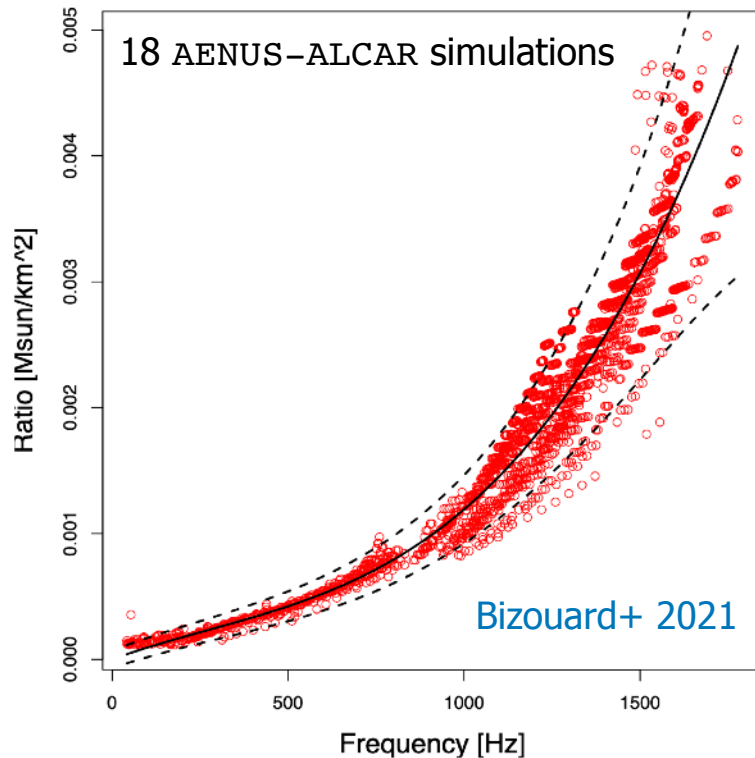
Detection prospects and inferences

Inference: method

We focus on the 2g_2 mode (main feature in spectrograms)

Goal: measure the time evolution of the ratio $r = \frac{M_{\text{PNS}}}{R_{\text{PNS}}^2}$ in GW data.

Step 1 of the method: Build a model that relates the ratio to the frequency evolution of the GW signal, $r(f)$, using 1D simulations (model set) and quasi-universal relations.



Discretized ratio parametrized with cubic polynomial regression

$$r_i = \beta_1 f_i + \beta_2 f_i^2 + \beta_3 f_i^3 + \epsilon_i$$

Errors take into account dispersion at high frequency. Zero-mean Gaussian error with variance σ_i

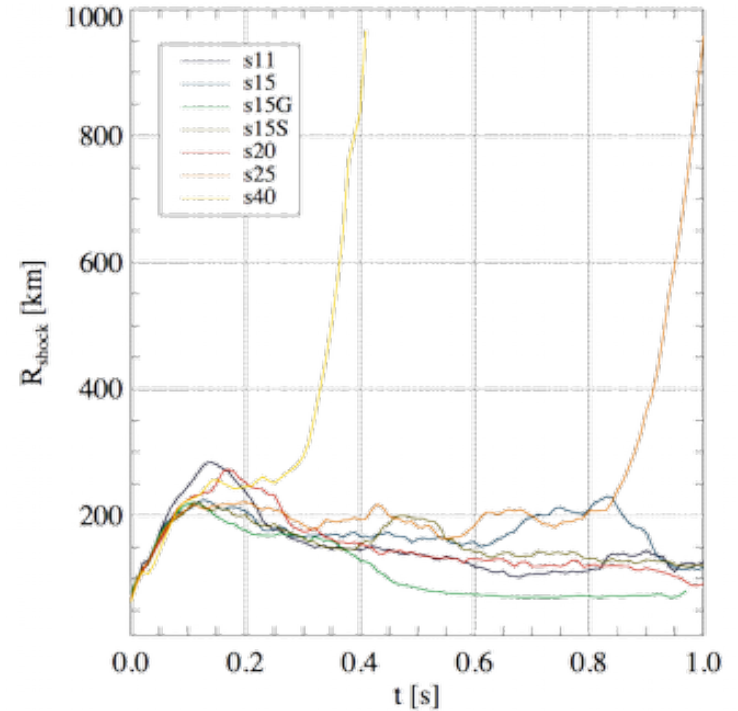
$$\log \sigma_i = \alpha_0 + \alpha_1 f_i + \alpha_2 f_i^2 + \delta_i$$

R-package `lmvar` to fit the model using maximum likelihood approach.

Inference: method

Step 2 of the method: Use 2D simulations (test set) for which $r(t)$ is known to validate model and provide detectability estimates.

Model name	M_{ZAMS} [M_{\odot}]	progenitor model	EOS	t_f [s]	$t_{\text{explosion}}$	$M_{\text{PNS},f}$ [M_{\odot}]
s11	11.2	[50]	LS220	1.86	×	1.47
s15	15.0	[50]	LS220	1.66	×	2.00
s15S	15.0	[50]	SFHo	1.75	×	2.02
s15G	15.0	[50]	GShen	0.97	×	1.86
s20	20.0	[50]	LS220	1.53	×	1.75
s20S	20.0	[51]	SFHo	0.87	×	2.05
s25	25.0	[50]	LS220	1.60	0.91	2.33
s40	40.0	[50]	LS220	1.70	1.52	2.23



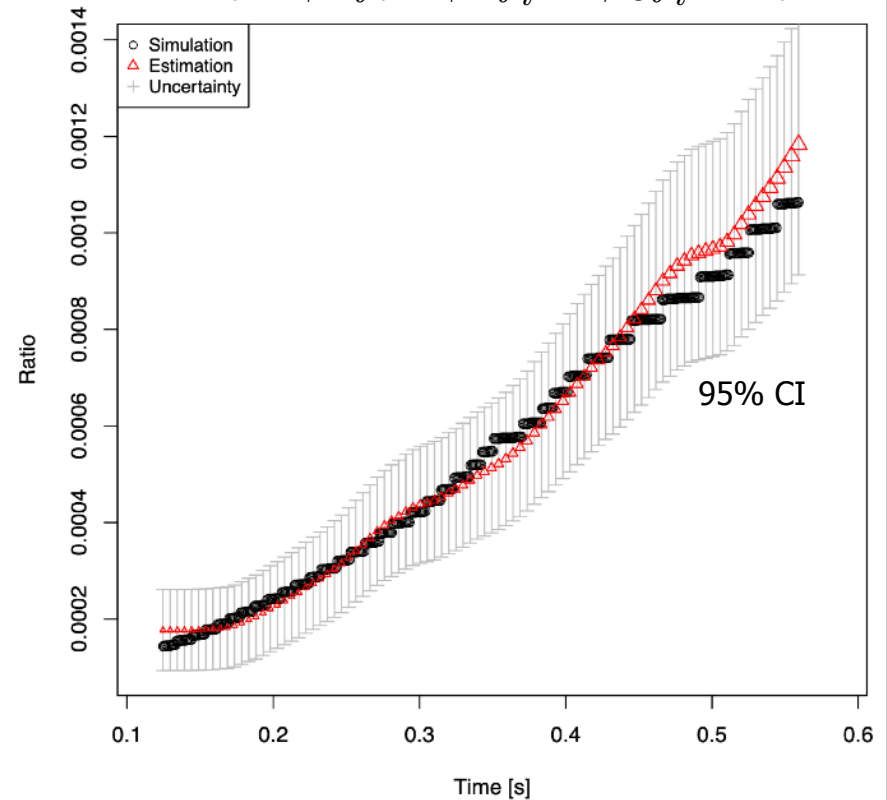
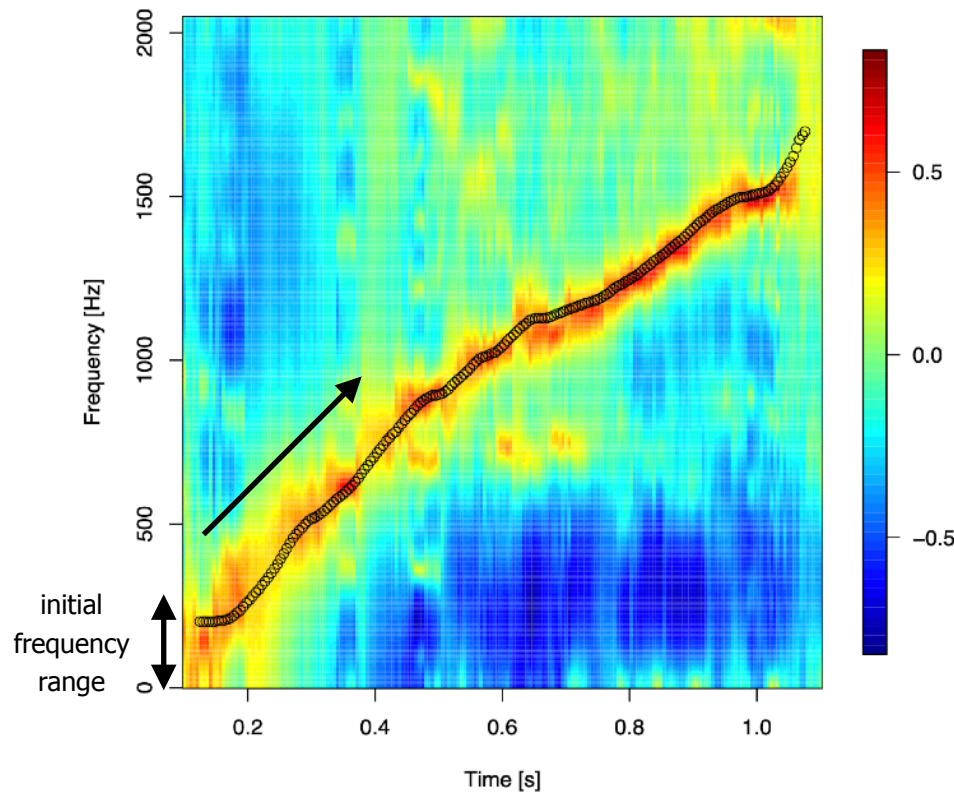
Inference: method

We compute the spectrogram and search for the 2g_2 mode frequency track (peak frequency using a simple track-finding algorithm)

- Starting frequency range: [0, 200] Hz
- Mode frequency can only grow

Example with s20S GW signal

$$r_i = \beta_1 f_i + \beta_2 f_i^2 + \beta_3 f_i^3 + \epsilon_i$$



Bizouard+ 2021

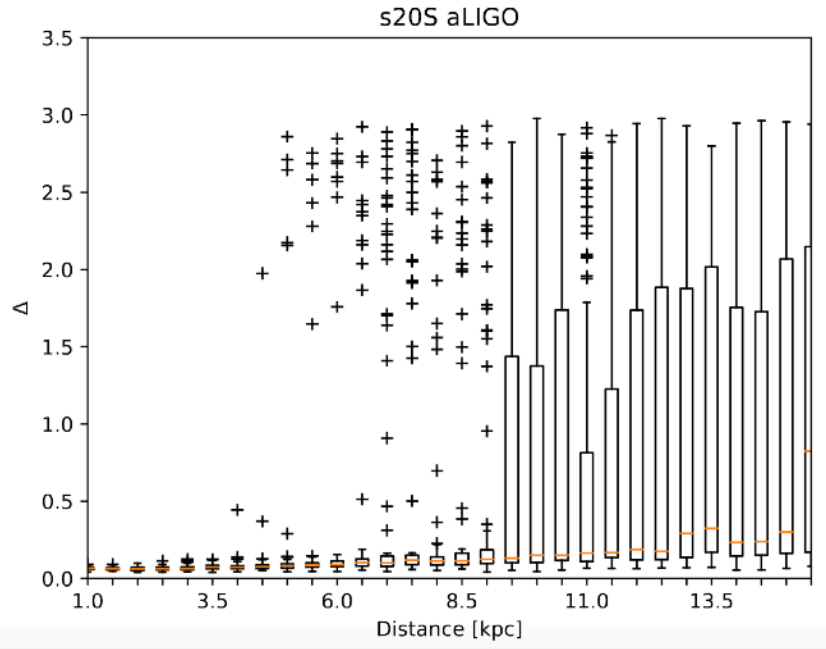
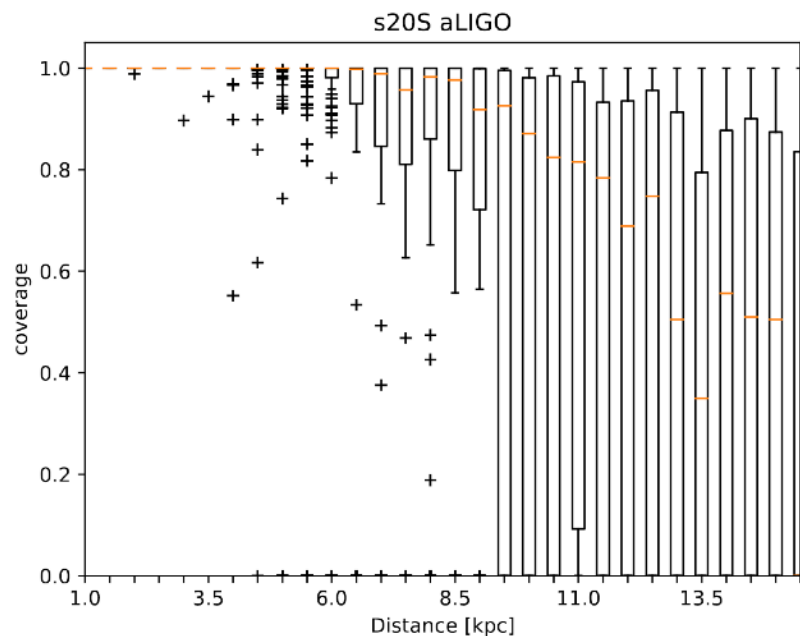
Detectability prospects: s20S waveform

Inject s20S GW signal into 100 Gaussian noise realizations (design Advanced LIGO PSD)

- Source optimally oriented wrt detector
- Assume CCSN GW signal has been identified in the data

Vary distance and compare reconstructed ratio to true ratio, using coverage (fraction of values within 95% CI) and relative error Δ

$$\Delta = \frac{1}{N} \sum_1^N \frac{|r_i - r_i^0|}{r_i^0}$$



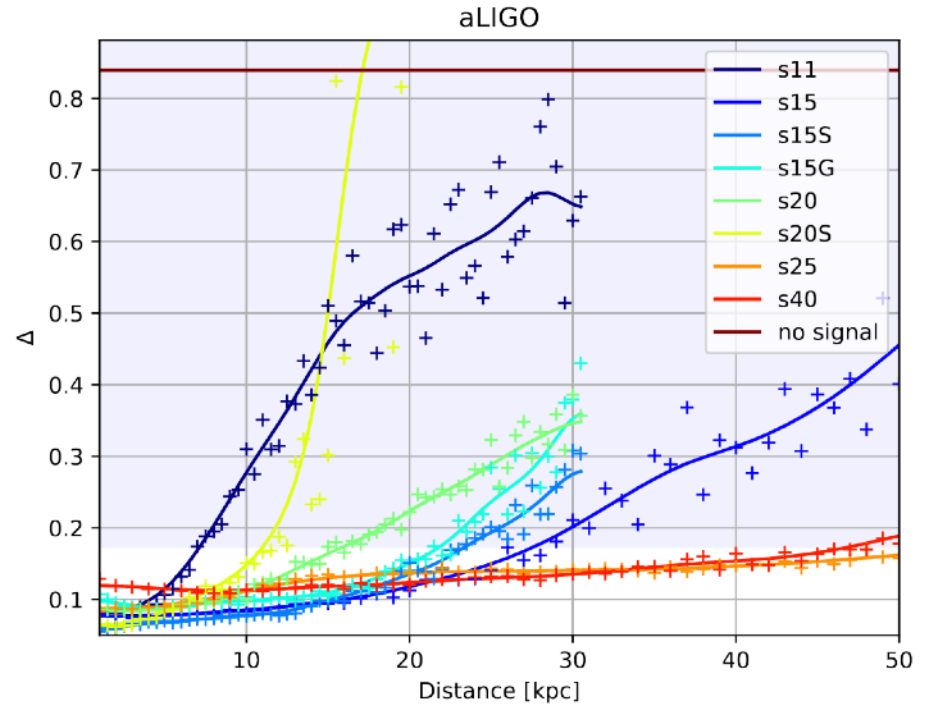
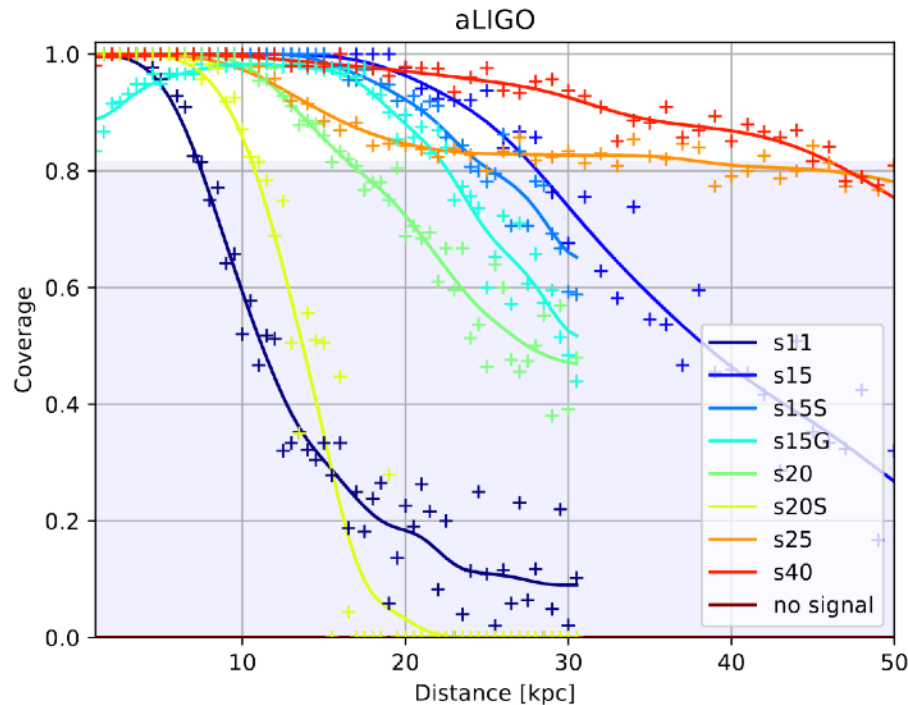
Bizouard+ 2021

Source at ~ 9 kpc: coverage $> 80\%$ and $\Delta < 20\%$

Detectability prospects: all waveforms

Test that the method does not depend on the waveform.

Performance: distance at which ratio can be reconstructed with a coverage $< 95\%$ of the noise-only coverage values.



Ratio well reconstructed for all waveforms (except s11 AND s20S) up to ~ 15 kpc.

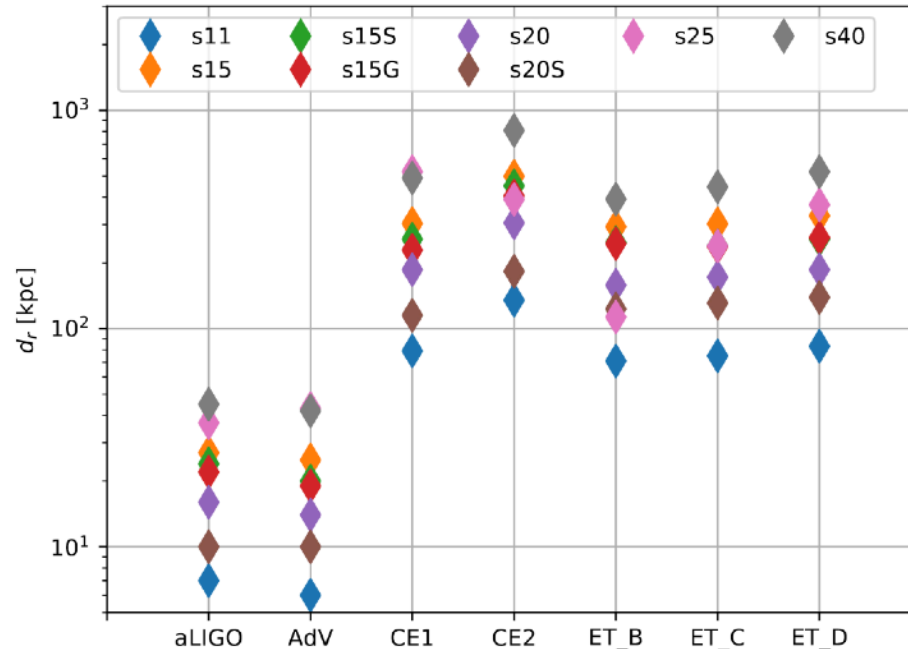
Coverage $> 80\%$ and Error $< 20\%$

Bizouard+ 2021

Detectability prospects: 2G and 3G detectors

Maximal distance at which the ratio $r = \frac{M_{\text{PNS}}}{R_{\text{PNS}}^2}$ is reconstructed with good accuracy for 2G and 3G detectors.

[Good accuracy = median of coverage < 95% of noise-only values]



Bizouard+ 2021

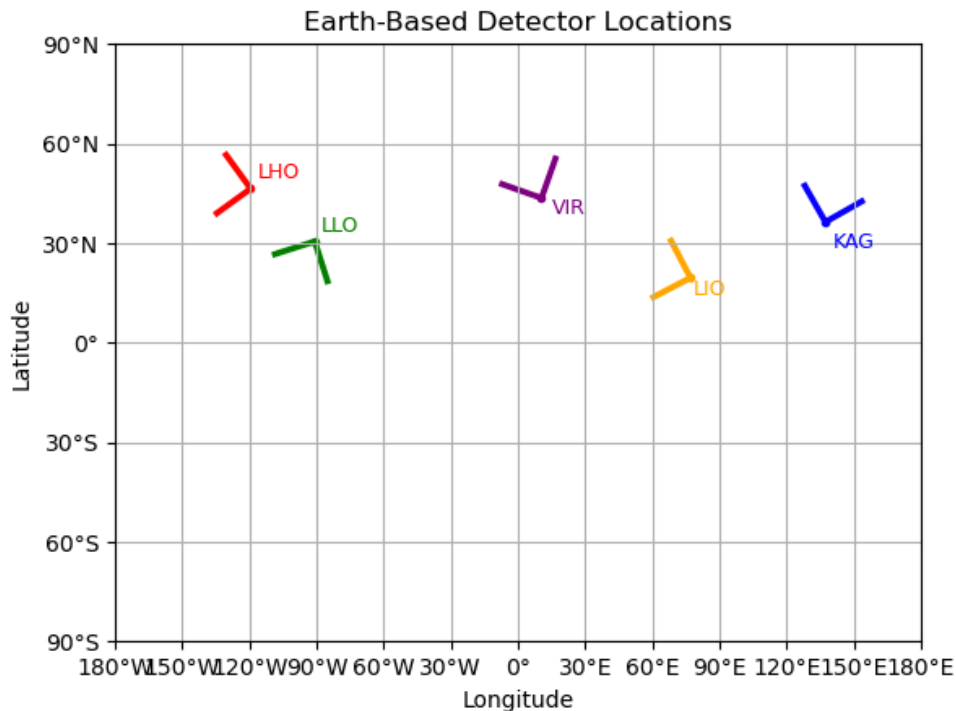
Cosmic Explorer and Einstein Telescope: [CE1, CE2: [Reitze+ 2019](#); ET_B, ET_C, ET_D: [Hild+ 2011](#)]

- Ratio reconstructed up to distance 100-700 kpc.

Multi-detector coherent analysis

Motivation: more realistic working case taking into account the sky position of the source and the location/orientation of each ground-based detector (Bruel+ 2023)

Location and orientation of ET and CE not yet known. For simplicity we locate ET at the location of the Virgo detector with arbitrary orientation. The two CE sites are set according to Borhanian (2021), where a 40 km detector is located in Idaho and a 20 km one in New Mexico.

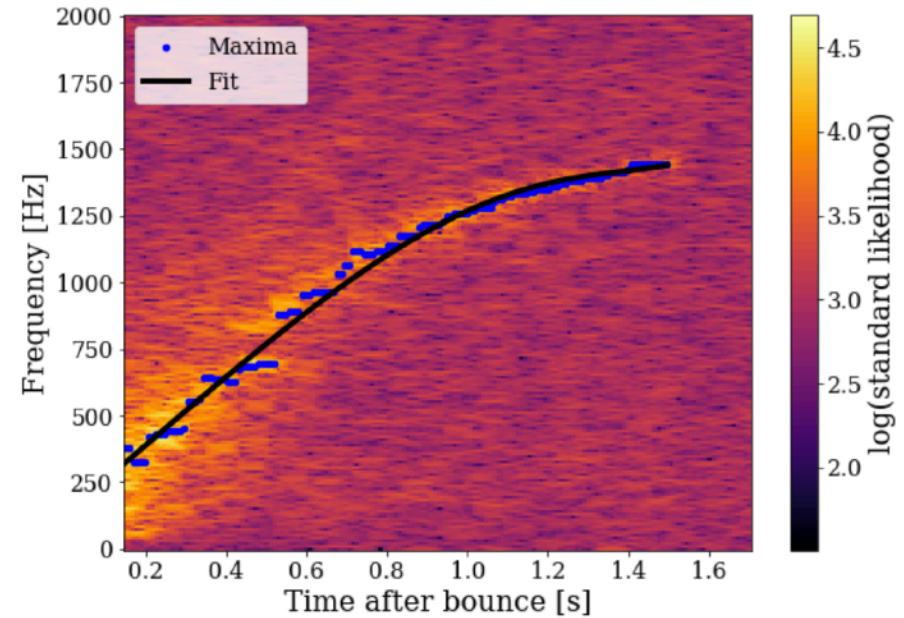
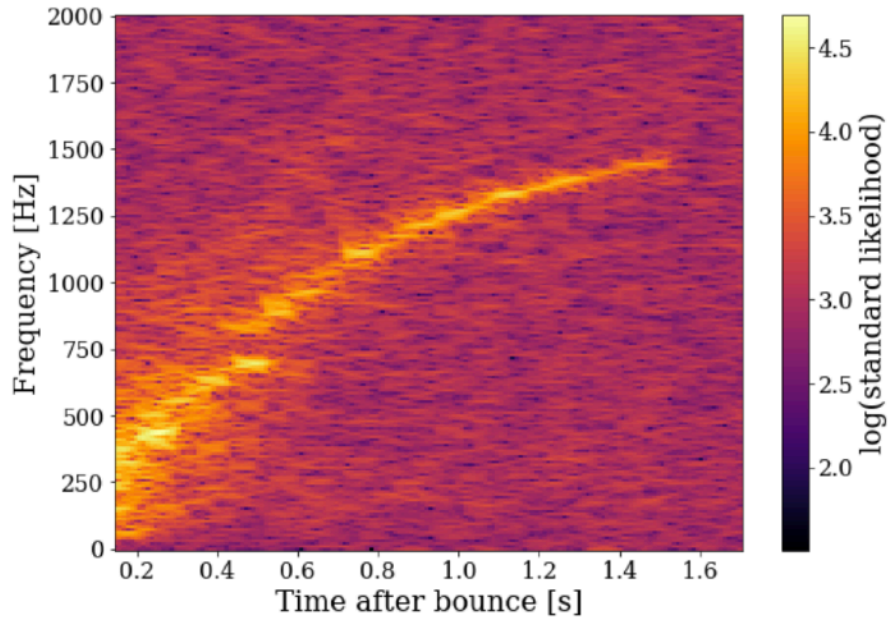


Network of 5 2G detectors (LHO, LLO, Virgo, KAGRA and LAO) at their nominal location and design sensitivity.

Credit: T. Bruel

Multi-detector coherent analysis

Coherent analysis of whitened data done following same method as in the X-pipeline (Sutton+ 2010)



Waveform: s20-LS220; Distance: 5 kpc
Detectors: LLO, LHO, Virgo, KAGRA

Signal track on spectrograms: LASSO fit
(polynomial regression) on maxima

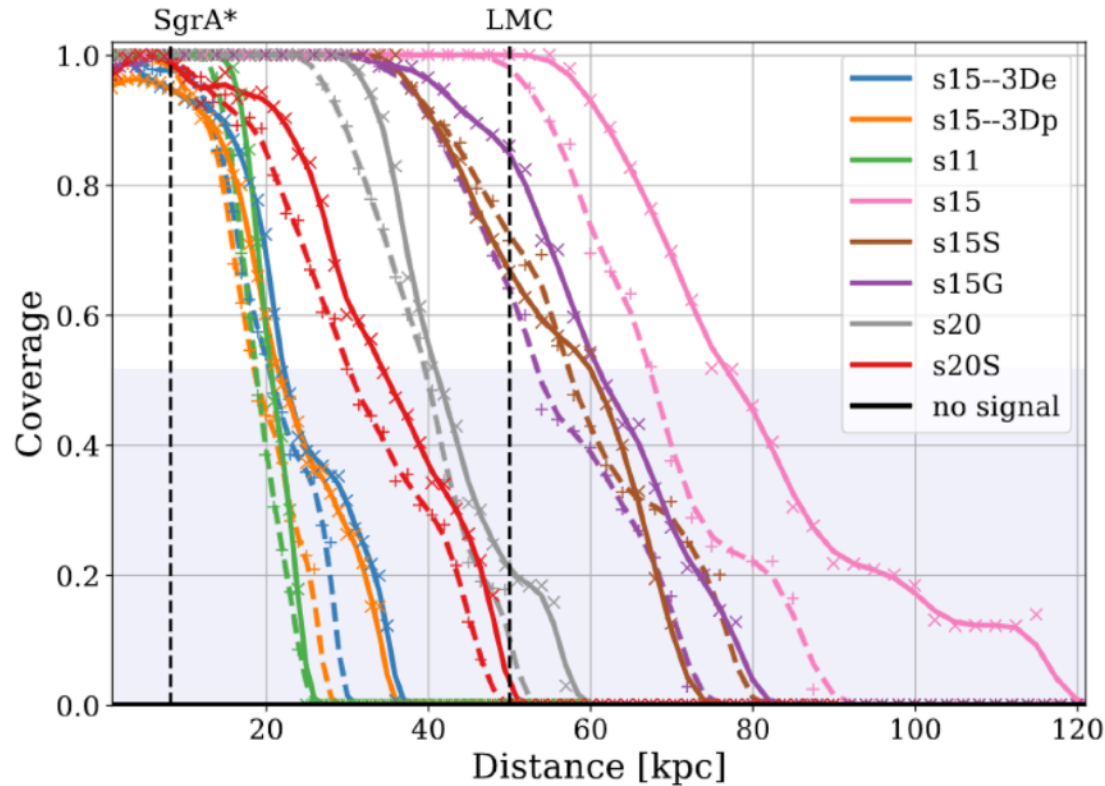
Bruel+ 2023

Performance - coverage evolution (2G detectors)

For a fixed source location (Sagittarius constellation) we vary the distance.

Solid lines: HLVKA network. Dashed lines: HL network

Brue+ 2023



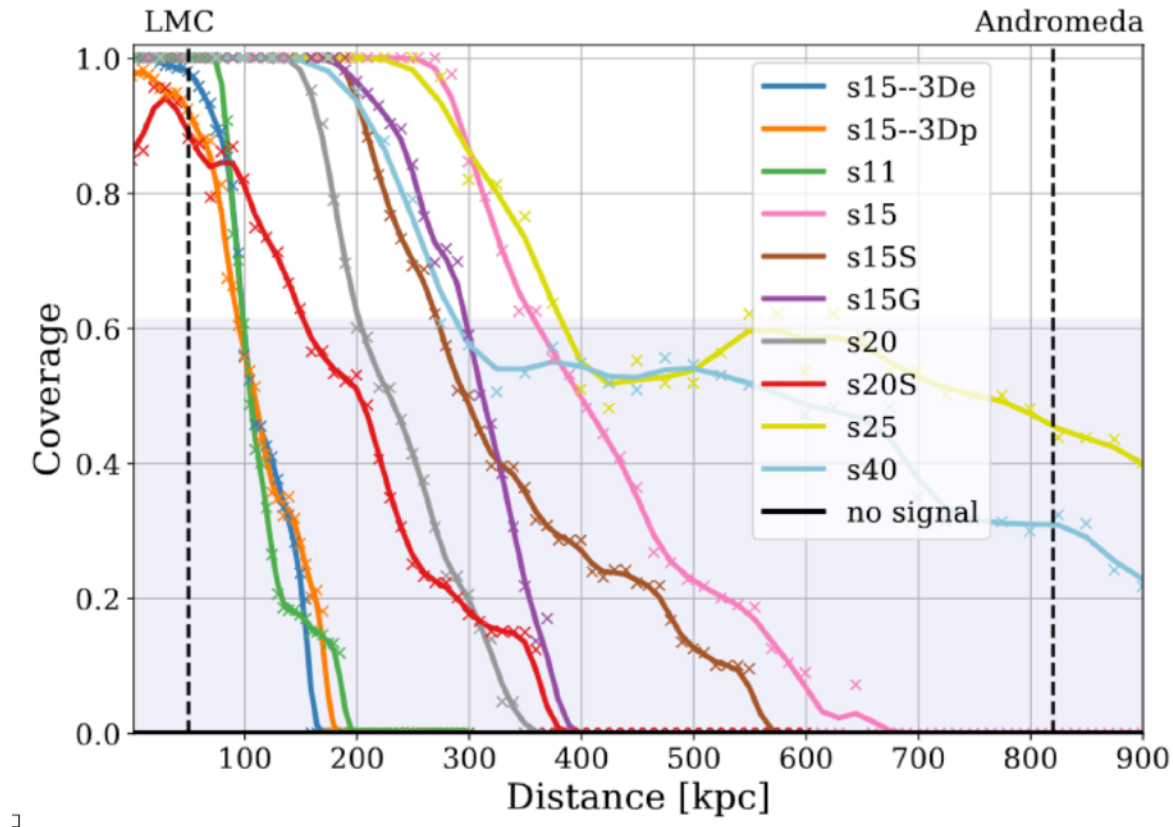
2G detectors at their design sensitivities able to measure $r = \frac{M_{\text{PNS}}}{R_{\text{PNS}}^2}$ of a Galactic CCSN for most of the progenitors considered in Brue+ (2023).

Performance - coverage evolution (3G detectors)

For a fixed source location (Andromeda) we vary the distance.

Bruel+ 2023

Solid lines: ET + CE20 + CE40 network.



A global network of the three third-generation detectors (CE20-CE40-ET) increases the distance reach to **several hundred kpc from Earth**.

Performance - 3G detectors

CCSN in nearby galaxies: Fraction of the coverage larger than 0.8 for arrival times of the GW spanning over a 24-hour period. Data correspond to s20 waveform.

Galaxy name	Distance [kpc]	RA [h]	dec [°]	CE20-CE40	ET	CE20-CE40-ET
Sagittarius	20	18.91753	-30.47833	0.96	0.92	1.0
Segue 1	23	10.11756	16.07361	0.92	0.92	1.0
Tucana III	25	23.94333	-59.6	0.96	0.83	1.0
Hydrus I	27.6	2.49261	-79.3089	0.92	0.88	1.0
Carina III	27.8	7.642	-57.89972	0.88	0.92	1.0
Triangulum II	30	2.22150	36.17844	0.88	0.88	1.0
Reticulum II	32	3.59503	-54.04917	0.88	0.84	1.0
Ursa Major II	34.7	8.85833	63.13	0.88	0.84	1.0
Segue 2	35	2.32111	20.17528	0.67	0.84	1.0
Carina II	36.2	7.60711	-57.99917	0.88	0.79	1.0
Coma Berenices	42	12.44972	23.90417	0.79	0.79	1.0
Boötes II	42	13.96667	12.85000	0.79	0.83	1.0
Willman 1	45	10.82250	51.05	0.79	0.79	1.0
Boötes III	50	13.95206	26.775	0.79	0.79	1.0
Large Magellanic Cloud	50	5.39294	-69.75611	0.75	0.75	1.0
Tucana II	58	22.86531	-58.56889	0.75	0.67	0.92
Small Magellanic Cloud	60	0.87722	-72.80028	0.67	0.71	1.0
Ursa Minor	60	15.15316	67.21436	0.71	0.71	0.92
Boötes	66	14.0000	14.5000	0.71	0.71	0.92
Draco	80	17.33732	57.92122	0.63	0.63	0.83

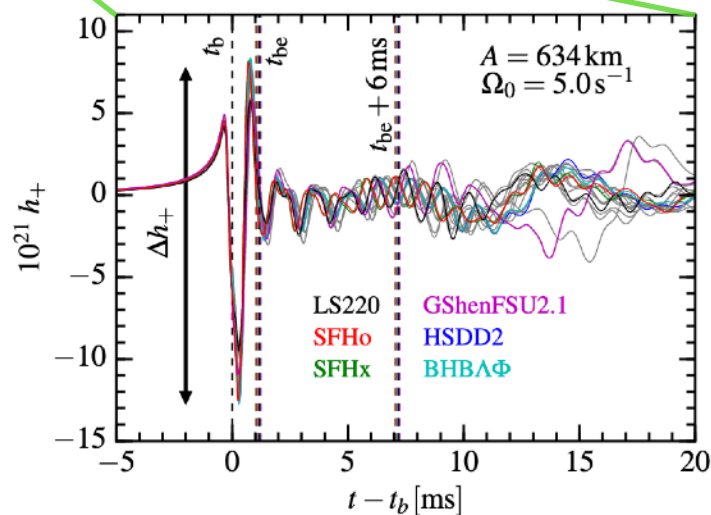
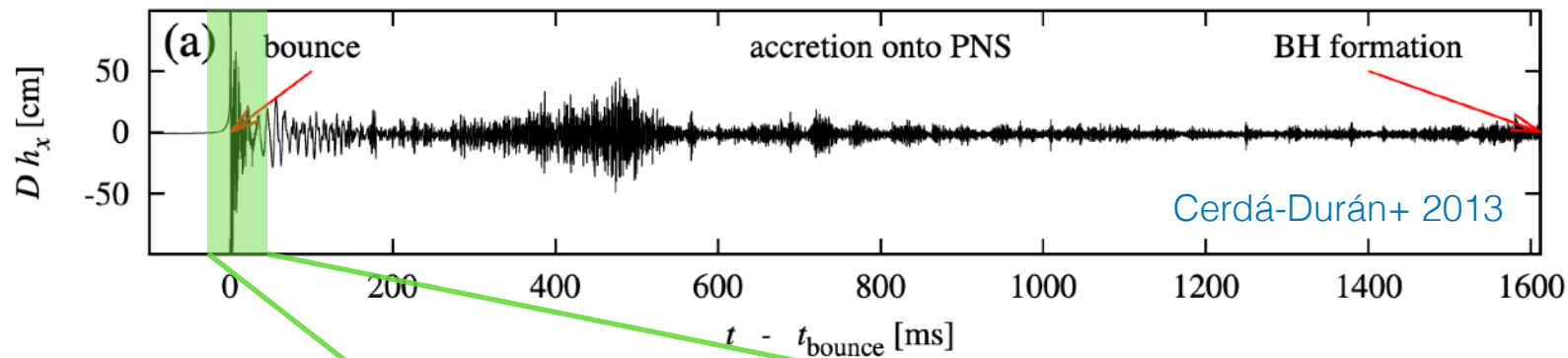
Bruehl+ 2023

Rapidly rotating progenitors

Inference with rapidly rotating CCSN

The **peak GW emission at bounce** is related to the degree of **oblateness** of the core at bounce, which is related to the **rotation rate**.

Most comprehensive study of the bounce signal done by [Richers+ \(2017\)](#): over 1800 2D CCSN simulations (up to 10ms post-bounce). Only one GW polarization (h_+) non-zero.

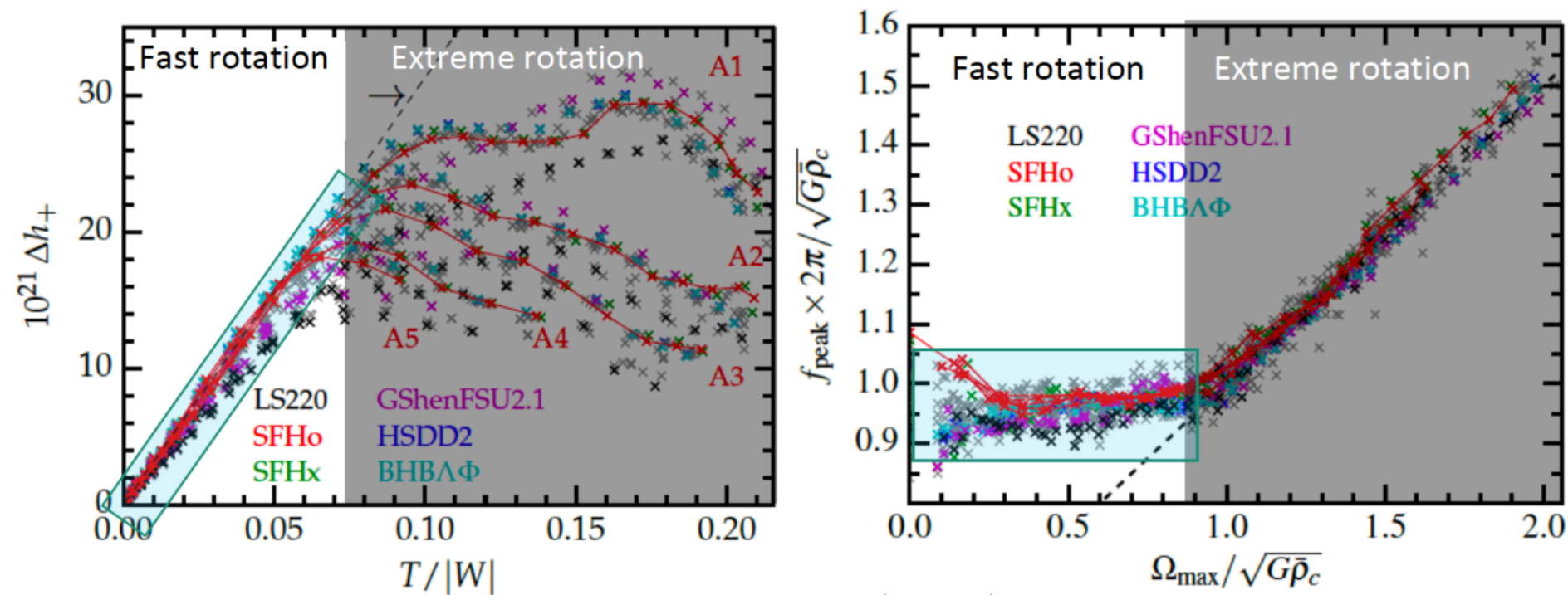


[Richers+ 2017](#)

Main features:

- Peak with amplitude Δh_+
- Several oscillations with frequency f_{peak}

Inference with rapidly rotating CCSN



Richers+ (2017)

$$\Delta h_+ \propto \frac{T}{|W|}$$

$$f_{\text{peak}} \propto \frac{1}{\sqrt{\rho_c}}$$

Q: What can we learn from performing PE on Δh_+ and f_{peak} ?

A: We can estimate the **source parameters**: ρ_c and $\frac{T}{|W|}$

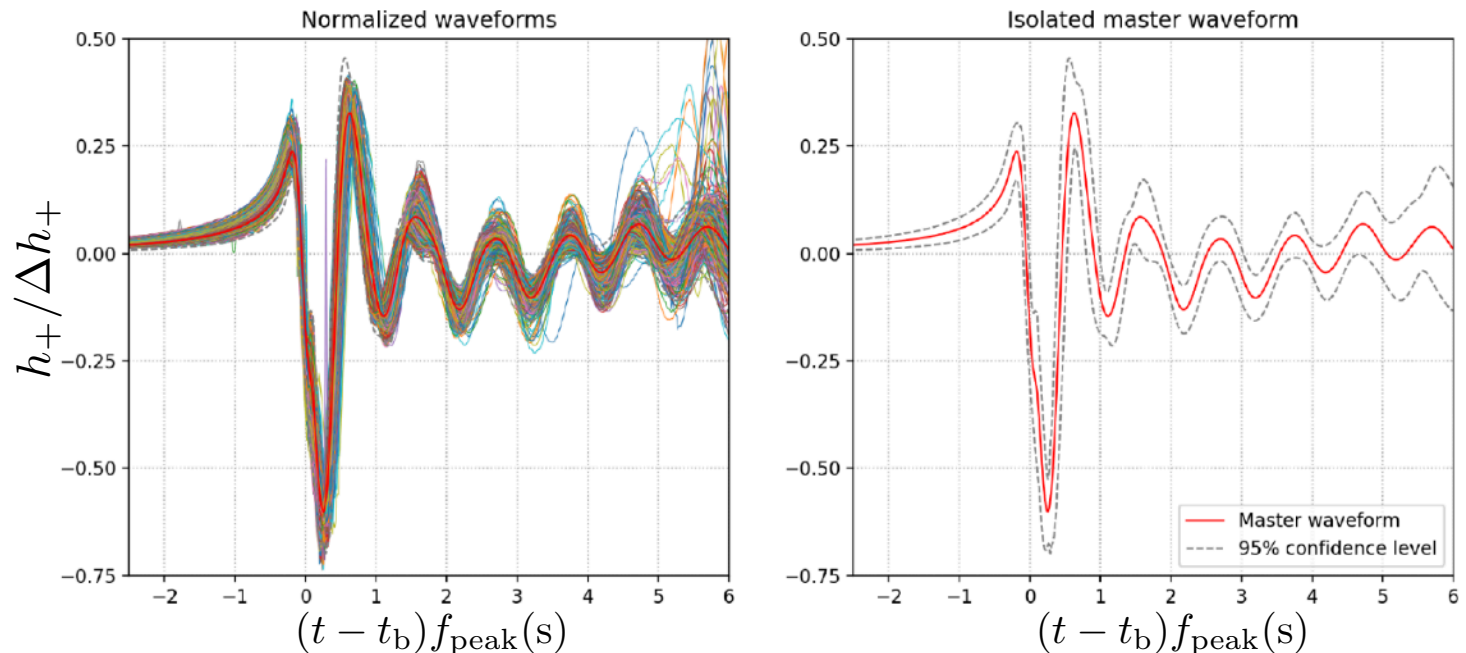
Inference with rapidly rotating CCSN

Possible to describe a large fraction of the [Richers+ \(2017\)](#) waveforms in the early post-bounce phase in a simple form - **a master waveform template** - depending only on Δh_+ and f_{peak}

Include only models that (a) collapse, and (b) $0 < \frac{T}{|W|} < 0.06$

Waveforms are: (a) aligned at time of bounce, (b) strain and time axes renormalized, (c) overlap late sinusoidal phase as much as possible.

Master waveform: average of 420 waveforms.



[Pastor-Marcos+ \(2024\)](#)

Inference with rapidly rotating CCSN

Waveform model depends on **three parameters**: $\Theta = \{D \cdot \Delta h \cdot \sin^2 \theta, f_{\text{peak}}, \psi\}$

Perform **four series of injections** under different conditions (random values of parameters):

- Null injections with zero amplitude: only noise reference (no signal)
- Master waveform injections with $f_{\text{peak}} \in [600, 1000]$ Hz and $D \cdot \Delta h_+ \cdot \sin^2 \theta \in [0, 700]$ cm
- Random waveform injections among the 402 waveforms selected to build master template
- Random waveform injections from 12 additional signals from CCSN simulations

Each series consists of 1000 injections on random Gaussian noise of a 3-detector HLV network at design sensitivity.

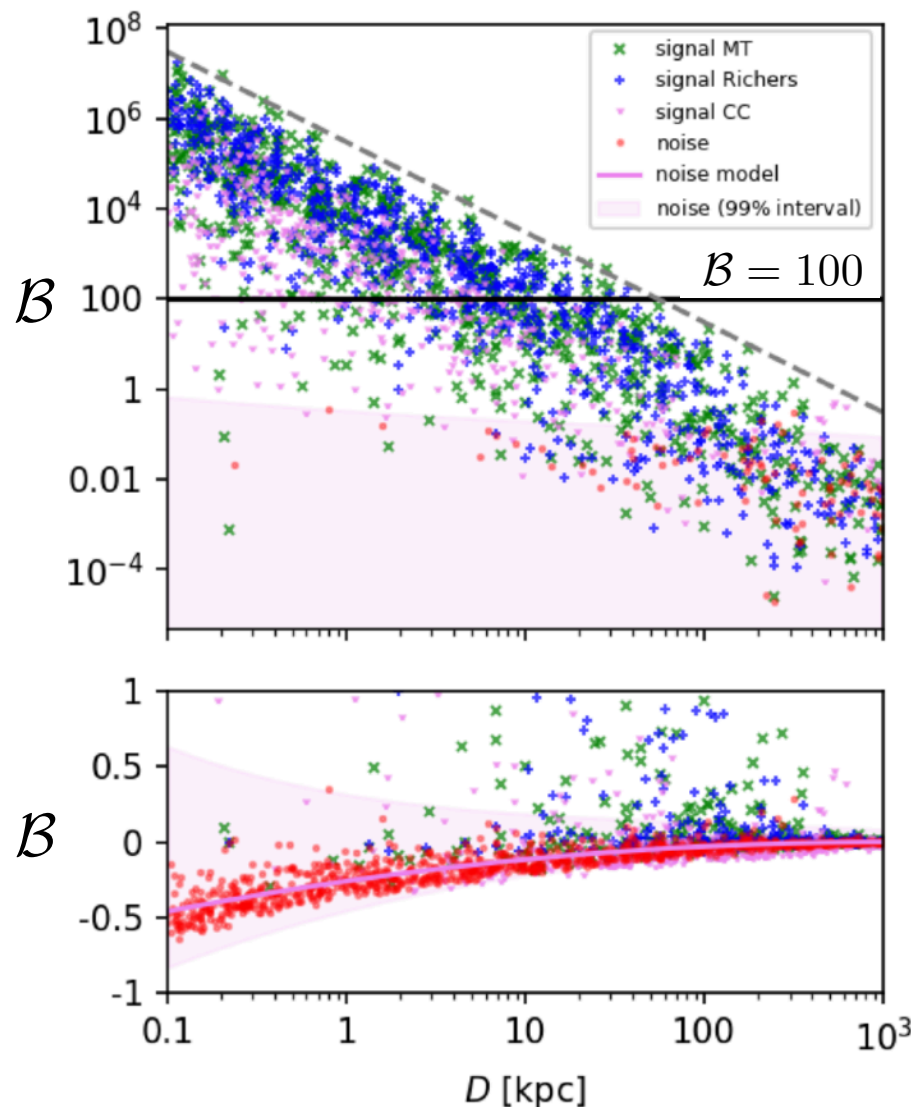
Injections performed at:

- Random sky location
- Random luminosity distance in 0.1-1000 kpc range
- Random inclination angle of rotation axis

For each injection, inference on the three parameters is performed, assuming source location in the sky, source distance, and time of bounce known.



Inference with rapidly rotating CCSN



Bayes factor: ratio of two competing statistical models represented by their evidence. Quantifies the support for one model (signal) over the other (noise).

For signal injections:

$$\max \text{ of } \log_{10} \mathcal{B} \propto \frac{1}{D^2}$$

For noise injections:

$$\log_{10} \mathcal{B} \approx 0$$

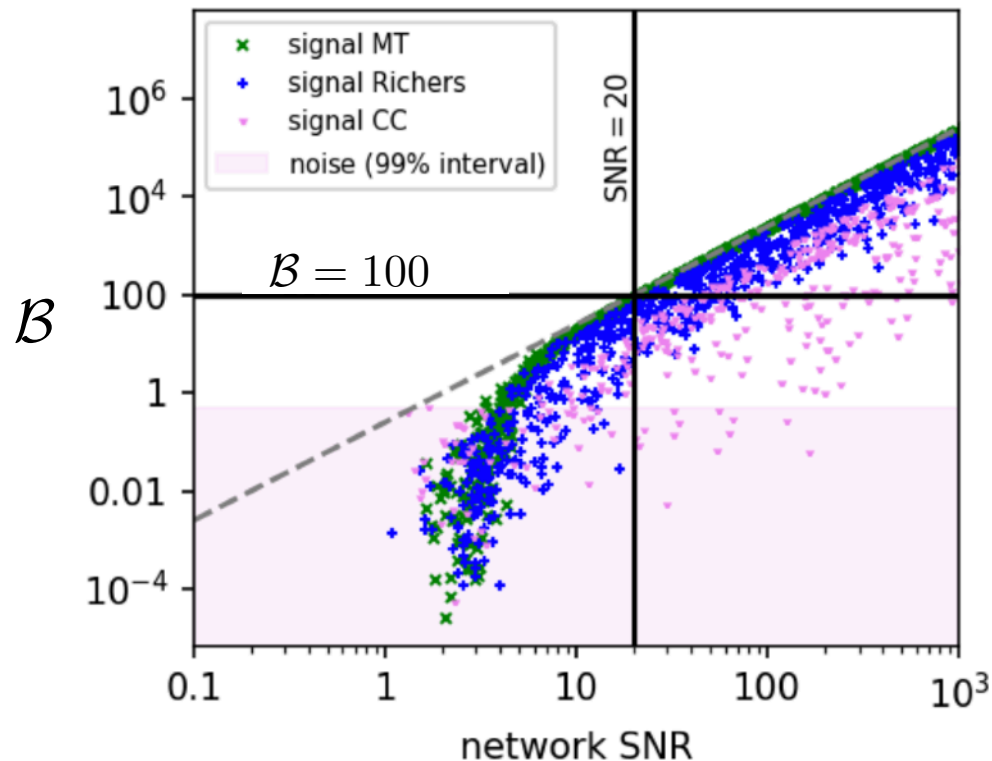
In general, signals with $\mathcal{B} > 0.5$ are above the noise (99% CI)

Pastor-Marcos+ (2024)

Inference with rapidly rotating CCSN

cWB pipeline: over 50% of fast-rotating CCSN with $\text{SNR} > 20$ are detectable in real detector noise conditions (Szczepanczyk 2018).

Dependence of Bayes Factor with network SNR



Max of $\log_{10} \mathcal{B}$ proportional to network SNR squared (dashed line).

$\mathcal{B} > 100$ injections have $\text{SNR} > 20$

44% of master waveform injections
48% of individual Richers waveform injections
32% of signals from different CCSN simulations

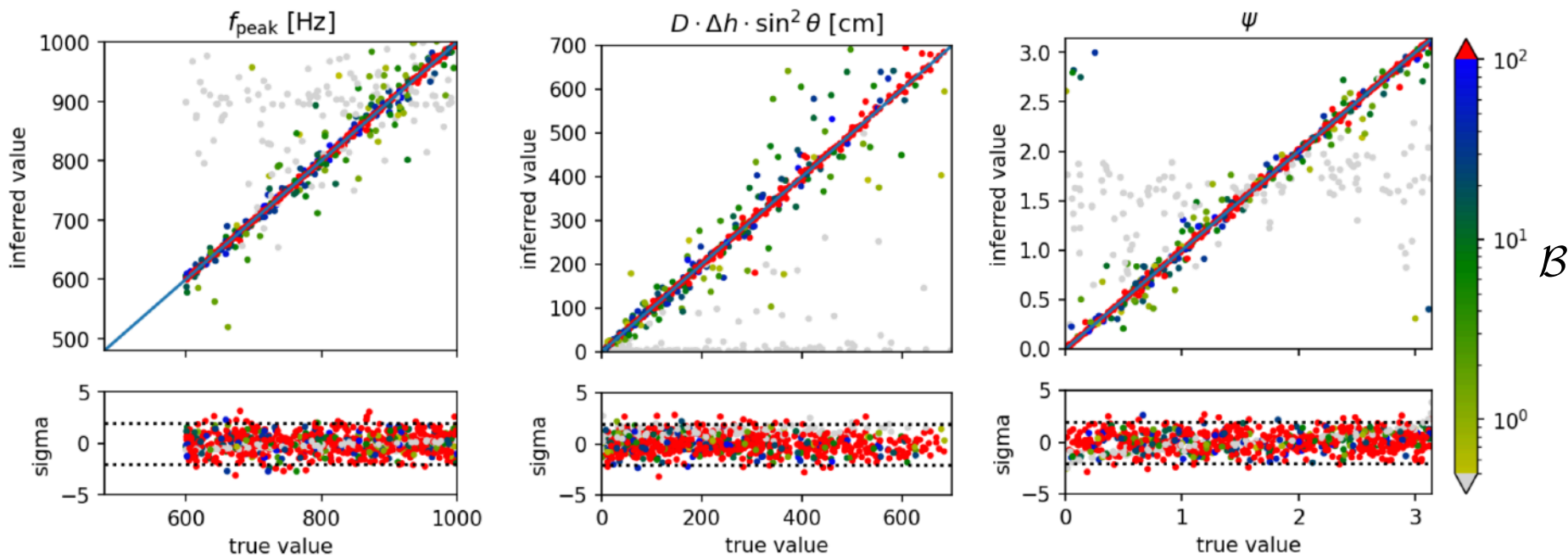
Conservative estimate of the potential detectability of a fast-rotating CCSN signal based only on observed data.

Pastor-Marcos+ (2024)

Inference with rapidly rotating CCSN

Master waveform injections.

Median of inferred posteriors vs true value of injected waveforms.



red $\mathcal{B} > 100$

grey $\mathcal{B} < 0.5$

→ Relative differences:

<2.3% f_{peak}

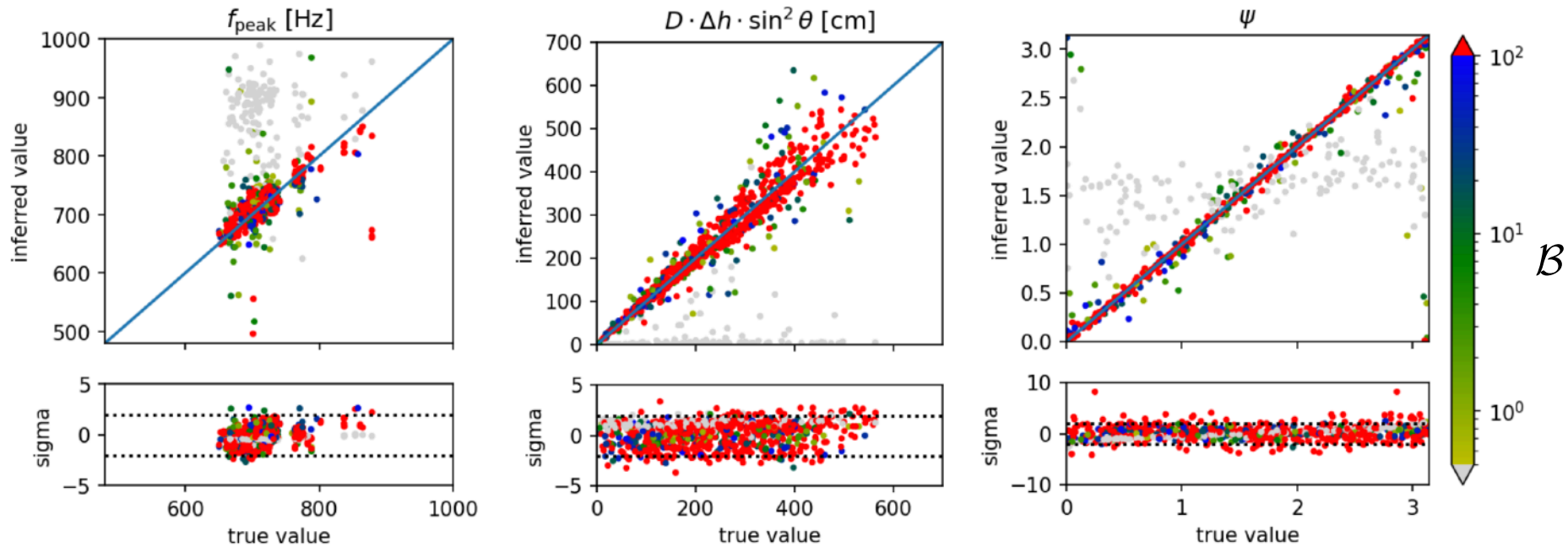
<14% $D \cdot \Delta h_+ \cdot \sin^2 \theta$

<7% ψ

Pastor-Marcos+ (2024)

Inference with rapidly rotating CCSN

Random waveform injections from Richers catalog
(master waveform does not perfectly match individual signals)

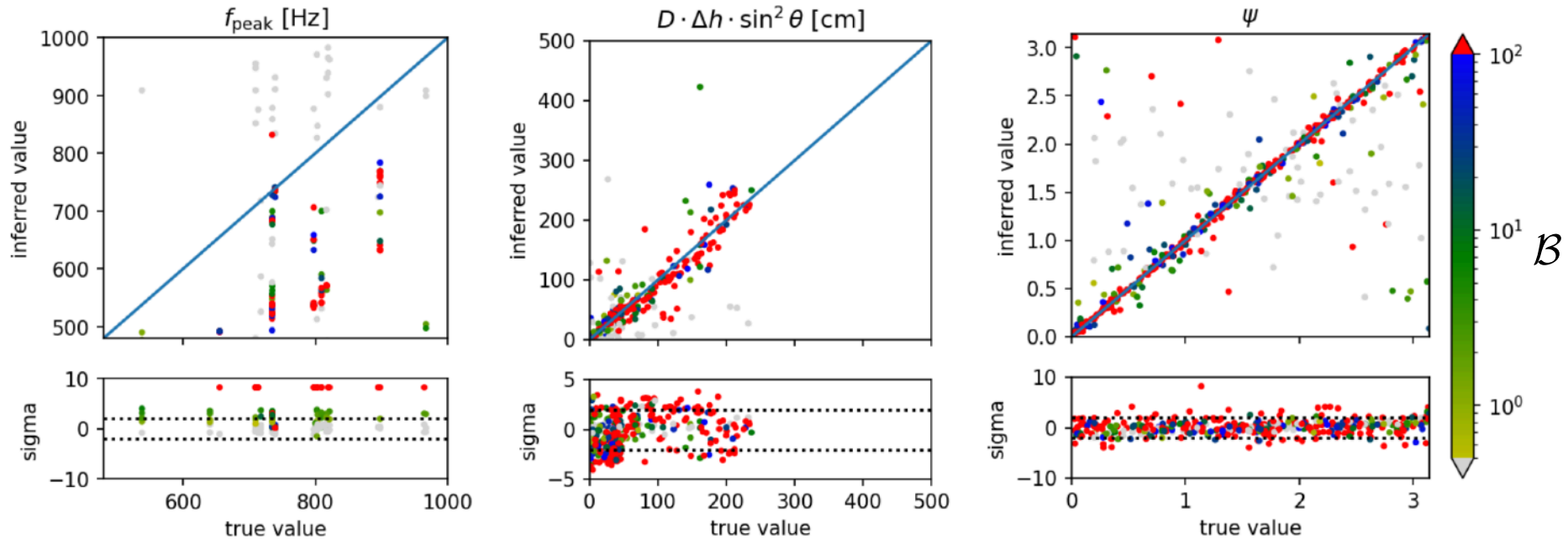


Larger dispersion of inferred values.

Pastor-Marcos+ (2024)

Inference with rapidly rotating CCSN

Random waveform injections from different CCSN signals



Clear mismatches between inferred and true values.

Underlying reason: post-bounce evolution of the 12 additional CCSN signals is more complex than those from Richers and cannot be modelled so faithfully by the master template waveform. Worst result for f_{peak} .

Pastor-Marcos+ (2024)

Summary

- CCSN are a prime source of gravitational waves.
- GW searches from CCSN always regarded as an essential activity in the LVK physics program.
- **Inference of PNS properties** using gravitational waveforms from CCSN may be **possible** in the future, following a successful detection.
- Illustrated with **two particular cases**:
 - Generic case (non-rotating CCSN, most common events)
 - Fast-rotating case (rare events)
- For generic CCSN, method based on the existence of quasi-universal relations between the frequency of oscillation of specific PNS modes and combinations of PNS parameters (mass and radius) and shock radius. **Asteroseismology of PNS.**
- For fast-rotating CCSN, a master waveform template can be built for the early bounce phase. Allows performing Bayesian inference on peak frequency and signal amplitude.